Journal of Radioanalytical and Nuclear Chemistry (2025) 334:5513–5526
https://doi.org/10.1007/s10967-025-10296-8

Sorption studies of cesium and cobalt in single and binary systems using Greek Petrota zeolite

Fotini Noli[1] · Lambrini Papadopoulou[2] · Natalia Palina[3] · Dieter Schild[3] · Frank Heberling[3] · Horst Geckeis[3]

Received: 27 March 2025 / Accepted: 18 July 2025 / Published online: 5 August 2025

Abstract

The sorption properties of a Greek zeolite for cesium and cobalt in single and binary systems were investigated. The sorption experiments were undertaken in aqueous solutions of pH 8, concentration range 10–500 mg L^{-1} and the metal concentration was determined by analytical (ICP-OES) and radiochemical techniques (γ-spectrometry using radiotracers of ^{137}Cs and ^{60}Co). Sorption isotherms in single and binary systems were reproduced by empirical and chemical models and the sorption capacity reached the theoretical maximum of 81.3 and 63.7 mg g^{-1} for Cs and Co respectively. The sorption process was studied through XRD, FTIR, autoradiography and SEM–EDS, whereas the environmental compatibility tests proved the safe sequestration of the loaded zeolite.

Keywords Cs and Co-uptake · Adsorption · Zeolites · Isotherms · Single and binary systems

Introduction

Natural zeolites are crystalline hydrated aluminosilicates and found in many types (*clinoptilolite, heulandite, chabazite*, *phillipsite*). They exhibit particular physical and chemical properties, such as enhanced adsorption and ion-exchange properties, resistivity, hydrothermal stability and selectivity. Therefore, they have a variety of applications, among them their use for radioactive waste immobilization and disposal. Due to their excellent adsorption properties and their ability for cation-exchange, working like a molecular sieve and they are useful in the removal of radioactive heavy metals from liquid nuclear waste [1–5].

As is known, nuclear power plants generate large amounts of intermediate and low-level waste containing the radioactive fission products ^{90}Sr and ^{137}Cs, and activation corrosion products such as ^{60}Co, ^{51}Cr, ^{63}Ni, ^{59}Fe, ^{65}Zn. Radiocesium (^{137}Cs) and radiocobalt (^{60}Co) are among the most important radionuclides in low-level radioactive liquid effluents generated from nuclear power plants because of their long half-life (30.17 years for ^{137}Cs and 5.27 years for ^{60}Co respectively), their high yield and toxicity. The importance of zeolites in engineered barrier systems and in geological disposal facilities as well as in environmental remediation after nuclear accidents has been widely demonstrated in the last decades [1, 2, 6–11].

In this work the sorption performance of Greek zeolitic rock from village Petrota in Evros (Northeastern Greece), was investigated in single and binary systems of Cs and Co aqueous solutions. The zeolites from Petrota have originated from the zeolitization process of volcanic ash that was possibly produced from the eruption of the Sheinovets caldera located in Bulgaria. Volcanic ash was transferred to its current location by water and under alkaline physicochemical conditions, the glass shards of the volcanic rocks were altered into zeolites [12, 13]. Zeolites present differences in the constitution and structure depending on the geographical areas of the mining and therefore in the case of their application, there is a need for additional study of their sorption behavior. The zeolites originated from this region present economic interest considering the reserves, the type and the zeolite content [13].

An attempt was made to study the Cs- and Co-adsorption on the raw Petrota zeolite (rock and powder form) combining sorption data and geochemical models as well

✉ Fotini Noli
noli@chem.auth.gr

[1] Radiochemical Lab., Department of Chemistry, Aristotle University, 54635 Thessaloniki, Greece

[2] Lab. of Mineralogy-Petrology, Department of Geology, Aristotle University, 54635 Thessaloniki, Greece

[3] Institute for Nuclear Waste Disposal (INE), Karlsruhe Institute of Technology (KIT), Karlsruhe, Germany

as autoradiography and SEM–EDS in radioactive and non-radioactive samples, considering the difference in mineral phases or elemental compositions. On the other hand, the prediction of competitive adsorption in binary systems is very challenging in the adsorption studies and to our best knowledge, data of simultaneous sorption of cesium and cobalt are very limited. Gutierrez and Fuentes for example studied the competitive sorption of cesium and cobalt onto montmorillonite and modified montmorillonites in binary systems as well as Park et al. [14–16]. The published data demonstrated the preferential Cs-uptake by clay minerals while Co-sorption seemed to be strongly affected by competition with cesium.

The current investigation was undertaken using the batch system and a variety of characterization techniques (XRD, FTIR, etc.) in order to explore morphological and structural changes of the zeolites and to obtain further insight into their sorption properties.

Experimental part

Materials and methods

The zeolite used for the sorption study was from Petrota region in Evros-Thrace, Greece [11–13]. Zeolites were sieved with 50 mesh, 250 mesh, and 500 mesh sizes while samples from the initial rock formation were also used.

The mineralogical composition of the zeolite was determined through powder X-ray Diffraction (pXRD) using a Philips PW 1710 diffractometer with Ni-filtered CuK_α radiation. The pulverized material was scanned with a step size of 0.0131º 2θ in the 2θ interval 5–70°.

BET surface area and volume were measured with an Autosorb-1MP, Quantachrome porosimeter via adsorption/desorption of nitrogen (77 K, partial pressure range P/P0:0.01–0.995) and after heating the samples under vacuum at 423 K. Furthermore, analysis utilizing the Attenuated Total Reflectance-Fourier Transform Infrared Spectroscopy (ATR-FTIR) in the range of 4000–400 cm^{-1} by a Thermo Scientific Nicolet iS20 spectrometer with a diamond reflectance crystal was performed.

The material was characterized before and after the sorption tests by Scanning Electron Microscopy/Energy Dispersive Spectroscopy (SEM–EDS) using the following setups: 1) JEOL JSM- 6390LV equipped with an Oxford INCA300 micro-analyzer, 2) FEI Quanta 650 FEG environmental scanning electron microscope (now Thermo Fisher Scientific Inc.). Material contrast images were obtained by a backscattered electron detector. SEM–EDS spectra of selected areas were acquired by use of a Thermo Scientific UltraDry (i.e. Peltier cooled, silicon drift X-ray detector and analyzed by Thermo Fisher Scientific Pathfinder software, version 2.11), 3) Electron microscope (EM), Energy Dispersive X-ray Spectrometry, including large area mapping (LAM) analysis using focused ion beam scanning electron microscopy (FIB-SEM)-Zeiss FIB-SEM, model CrossBeam 350 KMAT. The GEMINI objective lens generates a fine focused electron beam, with resolution of about 0.9 nm at 20 kV and beam current of 1.5 nA. Scanning Electron Microscope images were recorded using secondary electrons (Everhart–Thornley SE) detector. Energy Dispersive X-ray Spectrometry analysis was performed by a UltimMax100 (100 mm^2) silicon drift detector to determine elemental distribution and run a composition analysis of materials in SEM (SEM–EDS). The large LAM-EDS data acquisition, stitching of individual maps and data processing was done using AZtec 6.1 SP2 software by Oxfords Instruments. For LAM, accelerating voltage was set to 20 kV, single field of view was 2.33 mm by 1.75 mm with resolution of 1024 by 768 pixels, resulting in pixel resolution of 2.3 μm. Depending on the sample size the total number of fields varied between 60 and 120 fields.

Furthermore, distribution of radionuclides at the zeolite surfaces was analyzed using a Cyclone Storage System (Perkin Elmer) for digital autoradiography based on screens containing BaFBr:Eu^{2+} crystals.

Sorption experiments

For the sorption experiments we followed the procedure described in previous articles [11, 12]. All the reagents were of analytical grade (Merck, Darmstadt, DE). A water purification system (Millipore) with Elix and Milli-Q was used to provide ultra-pure water. As it is also derived by the code MEDUSA, Cs- and Co-ions are in the form of positively charged species in a large pH region (Cs^+ up to pH 12, Co^{2+} up to pH 8.5) [17]. After preliminary experiments in different pH values, it was decided to perform the sorption study at the optimum pH 8 [12]. The pH of the solutions was adjusted by adding NaOH or HCl solution dropwise and was measured using a pH meter (coulb glass electrode), and the calibration was performed at ambient conditions with standards buffers at pH 4, 7 and 9. Batch experiments were carried out by contacting 10 mL of the individual solutions (concentration 10–500 mg L^{-1}) with the adsorbent (dosage 1.0 g L^{-1}) for 24 h at ambient temperature (ca. 295 K). Kinetic experiments showed that the contact time was sufficient to establish a sorption equilibrium. The effect of competing ions was also studied using metal solutions with 0.05 M $Ca(NO_3)_2$ as background electrolyte. At the end of the experiments and after the separation of the solid from the liquid phase by centrifugation (Megafuge 2.R-Thermo Scientific) at 4000 rpm for 30 min, the equilibrium pH of the supernatant solutions was measured.

The Co- and Cs-aqueous solutions were prepared using solutions of analytical grade $CoCl_2$ and $CsNO_3$ in concentration range 10 to 500 mg L^{-1}. The radioactive standard solutions were ^{60}Co (in 0.1 M HCl supplied by Eckert & Ziegler Nuclitec GmbH) and ^{137}Cs (in 0.1 M HCl supplied by EUROSTANDARD CZ s.r.o.).

The cesium and cobalt concentrations were determined by gamma-ray spectrometry (CANBERRA HPGe detector with 23% efficiency and resolution 1.9 keV for the 1332 keV ^{60}Co gamma-radiation) via ^{137}Cs as tracer using the diagnostic photon energy of 661.6 keV and ^{60}Co at 1332 keV respectively. For construction of the sorption isotherms analytical ICP-OES (Optima DV 8300 by *PerkinElmer*) was also applied to determine the release of Na, Ca and Fe in the solution and the cobalt concentration.

The experiments took place twice with relative uncertainty of the measurements less than 5%. The average was used to calculate the adsorption capacity (q_e) by Eq. (1).

$$q_e = \left[\frac{C_i - C_e}{m}\right] \times V \quad (1)$$

where, C_i and C_e (mg L^{-1}) represent the sorbate concentrations in solution before and after sorption, V (mL) is the volume of the solution and m (mg) is the mass of the sorbent.

The experimental data were used to calculate the Cs- and Co-uptake and construct the corresponding isotherms which describe the equilibrium relationship between the sorbate and the sorbent at a specific temperature. Moreover, theoretical analysis using the Langmuir and Freundlich mathematical models was performed to assess the nature of the sorption.

The empirical Langmuir model (Eq. 2) assumes a localized monolayer adsorption on a fixed number of adsorption sites of equal energy (homogenous sorption) whereas the Freundlich model (Eq. 3) is based on a heterogeneous energy distribution on the surface not reaching a limited sorption capacity [18–22].

Langmuir equation (L)

$$\frac{C_e}{q_e} = \frac{1}{K_L q_{\max}} + \frac{1}{q_{\max}} C_e \quad (2)$$

Freundlich equation (F)

$$\ln q_e = \ln K_F + \frac{1}{n} \ln C_e \quad (3)$$

The q_e and C_e in the above equations are the equilibrium metal concentrations in the solid (mg g^{-1}) and liquid (mg L^{-1}) phase, respectively, q_{max} is the maximum sorption capacity (mg g^{-1}), K_L and K_F are the Langmuir and Freundlich equilibrium constants and n, in the case of Freundlich equation, is a parameter characterizing the system heterogeneity.

Desorption experiments

The environmental compatibility of the sorbents after loading was assessed by the Toxicity Characteristic Leaching Procedure (TCLP, U.S. EPA Method 1311) [23]. Desorption studies were conducted using Extraction Fluid #1 (5.7 mL glacial CH_3COOH and 64.3 mL of 1 mol L^{-1} NaOH successively added to distilled water subsequently diluted to a total volume of 1 L) in contact with 20 mg of the appropriate adsorbent, after loading it with 500 mg L^{-1} solution of Cs^+ and Co^{2+} respectively and shaking for 18 h.

Results and discussion

Surface characterization

The Petrota zeolitic rock samples contain mainly HEU-type (heulandite-clinoptilolite) zeolite (89%) with small amounts of mica, quartz, feldspars and clay minerals. This is demonstrated in powder XRD pattern in Fig. 1, where the characteristic clinoptilolite diffraction peaks at 2θ = 9.80, 11.12, 22.36, 29.94° corresponding to the (020), (200), (400), (151) planes can be seen [12, 24, 25]. Small cristobalite crystals were also present. Interaction with Cs-solution caused some differences in the XRD diffractogram at 25–35° which could be attributed to ion exchange of Cs-ions as reported by other researchers [8, 11, 24, 25]. Small changes are also caused after the interaction with Co- or Cs/Co-solution at 10° and at 22–23° respectively. Characteristic properties of zeolite such as cation exchange capacity (CEC), point of zero charge (pH_{pzc}) and BET surface area (S_{BET}) and volume (V_{BET}) as well as micropore surface area (S_{micro}) and volume (V_{micro}) are given in Table 1 along with the chemical composition obtained by SEM–EDS [12, 26]. As known sorption

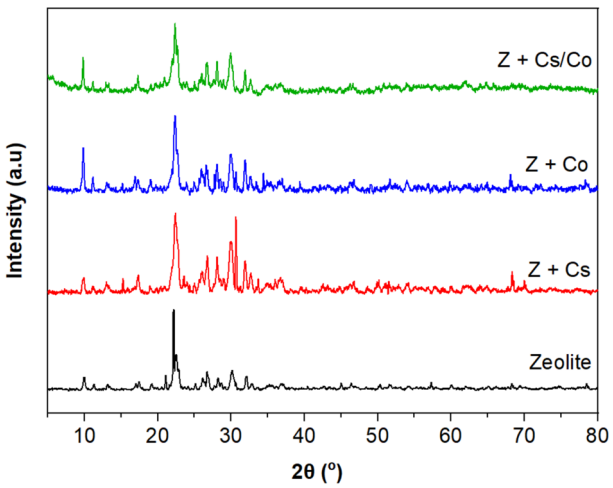

Fig. 1 pXRD diffractograms of zeolite before and after sorption

Table 1 Characteristic properties of zeolite

Material	S_{BET}(m^2/g)	S_{micro}(m^2/g)	V_{BET}(cm^3/g)	V_{micro}(cm^3/g)	pH_{pzc}	CECmeq/100 g	
Powder	32	9	0.106	0.004	7.7	217	
Composition (weight %)	Na	Mg	Al	Si	K	Ca	Fe
Powder	0.92–2.9	0.65–1.07	4.14–24.1	1.20–41.7	1.4–3.5	1.04–2.63	6.77–33.1
Rock	0.2–2.3	0.12–4.9	4.2–16.8	1.2–41	1.2–3.3	1.5–6.3	1.1–7.8

capacity is strongly affected by the high cation-exchange capacity, surface area, and porosity [25]. The Petrota zeolite is characterized by high CEC, surface area, and porosity [25, 26].

The FTIR spectra of the zeolite before and after sorption are presented in Fig. 2. A typical zeolite pattern is observed for the pristine material [27, 28]. The broad band around 3400 cm^{-1} is due to stretching O–H vibrations while the band at 3616 cm^{-1} is attributed to surface Si–OH and Al–OH groups of the zeolite lattice and the band at 1630 cm^{-1} to the bending O–H vibrations. The characteristic aluminosilicate bands at 1005, 792, and 585 cm^{-1} correspond to the asymmetric stretching vibrations of both the zeolitic tetrahedra (T–O–T) and similar vibration modes of mineral impurities (quartz, feldspars), as well as the symmetrical stretching vibrations of O–T–O bonds, and vibrations associated with the pore structure of HEU-type zeolites. The interaction with Co-solution results in some differences in the FTIR spectrum. The new band at 1380 cm^{-1}, is probably assigned to the lattice vibrations and to the excess alumina in the pores [29]. The band at 588 cm^{-1} is shifted to higher wavenumbers, while the main band at 1029 cm^{-1} shows a tendency to split into two new peaks. Similar observations have been reported by Sobalík et al. in their study concerning the presence of transition metal ions in zeolites [30]. The splitting of the main band can be attributed to the binding of Co^{2+} ions to framework oxygen atoms resulting to perturbation and deformation of the T–O–T bonds and to a different vibration frequency. The splitting into two separate bands indicates different cobalt-oxygen bonding strengths, or different cobalt-binding sites in the framework [31, 32]. Few differences were observed in the spectrum after interaction with CoCs-solution and even fewer in that of Cs-sorption.

Sorption study

The effect of the particle size of the powder material on the Cs-retention is shown in Fig. 3 (grain size: 500–250 µm and less than 50 µm) where can be seen that the smaller grain size the higher uptake because smaller size results in greater

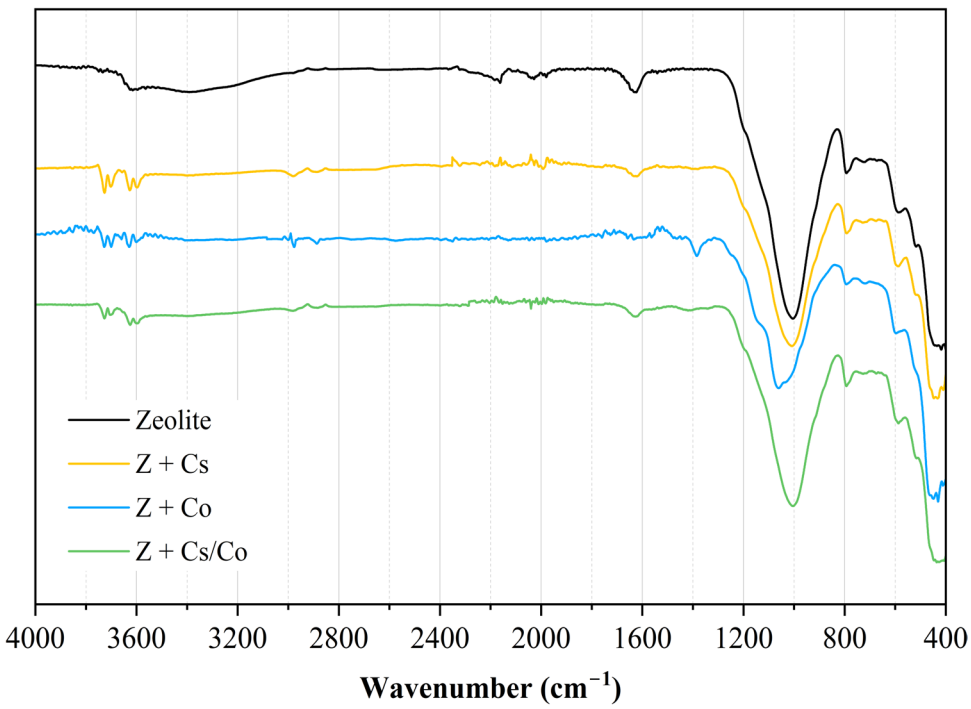

Fig. 2 FTIR spectra of zeolite before and after sorption

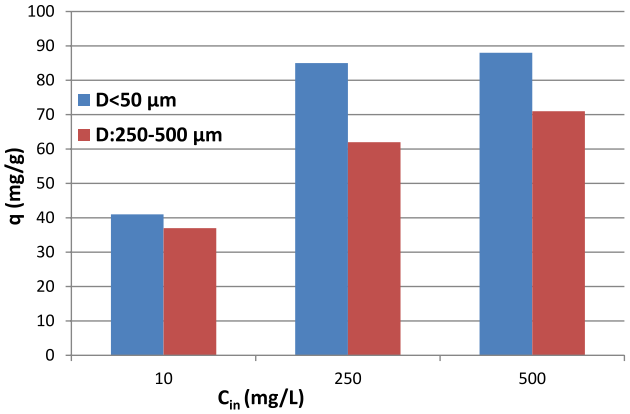

Fig. 3 Cs-sorption capacity onto zeolite according to particle size

specific surface area which means more active sites for sorption [33]. For the sorption experiments, samples with grain size < 50 µm were used.

The effect of contact time on Cs- and Co-sorption on zeolite is illustrated in Fig. 4 demonstrating that the adsorption proceeds very fast, and the equilibrium is achieved in less than 30 min which is characteristic of ion exchange process. This is also indicated by the pH_{equil} which was reduced by about one unit.

The uptake data of Cs-sorption onto zeolite according to the equilibrium metal concentration in Cs-solution as well as the corresponding results for Co-sorption are illustrated in Fig. 5.

Adjustment of the experimental data to Langmuir and Freundlich models confirmed as it is shown in Table 2, that the best fitting was to Langmuir model for the Cs-sorption indicating monolayer coverage (homogenous adsorption). In the case of Co-sorption, the data are better described by

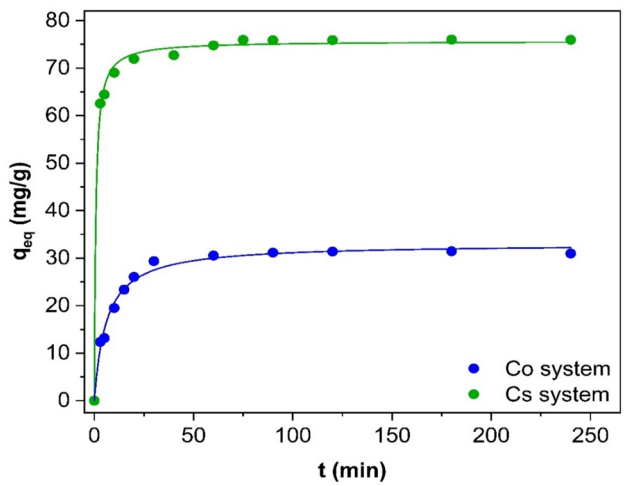

Fig. 4 Effect of contact time on Cs- and Co-sorption on zeolite (C_i: 250 mg $L.^{-1}$, T: 295 K)

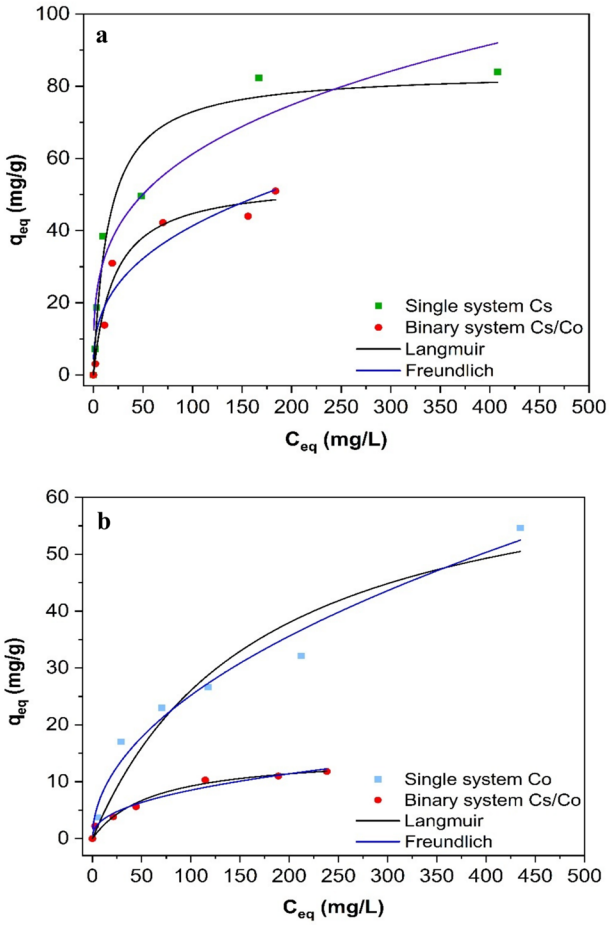

Fig. 5 Sorption isotherms of (**a**) cesium and (**b**) cobalt onto zeolite in single and binary system (pH 8, T:295 K)

Freundlich isotherm indicating surface heterogeneity and multi-layer adsorption [6, 12, 34].

The corresponding isotherms for Cs- and Co-sorption in binary system (1:1 Cs/Co solution) are also illustrated in Figs. 5a and b where it is shown that the adsorption capacity of cesium was suppressed from 80 to 50 mg g^{-1} in 1:1 Cs/Co solution. Co^{2+}-ions act as competing ions occupying the available sorption sites and decrease the adsorption capacity of cesium (circa 38%) while the corresponding adsorption capacity of cobalt was significantly decreased (circa 63%) in presence of Cs^{+}-ions in binary system. Similar observations have been reported by other researchers studying the sorption of cesium and cobalt in single and binary systems. Gutierrez and Fuentes investigated the adsorption of cesium and cobalt onto Ca-montmorillonite in binary systems and observed that the Cs-sorption was less affected by Co-sorption, which is consistent with the preferential uptake of cesium by clay minerals [14]. Park et al. also observed the predominant Cs-sorption onto montmorillonite and modified montmorillonites versus Co-sorption [15, 16].

Table 2 Parameters of the Langmuir and Freundlich models for Cs- and Co-sorption in single systems

	Langmuir model			Freundlich model		
	K_L (L mg^{-1})	q_{max} (mg g^{-1})	R^2	K_F (mg/g)(L/mg)$^{1/n}$	1/n	R^2
Cs-sorption	0.06914	81.3	0.9953	9.9682	0.3920	0.8489
Co-sorption	0.00819	63.7	0.8958	1.7977	0.5695	0.9126

From the ICP results it was also found that after sorption the concentrations of released Na- and Ca-ions in Cs-solutions were higher, followed by binary Cs/Co-solutions and single Co-solutions. The opposite phenomenon was observed for the Fe-concentration.

These results demonstrate that cesium ions replace the sites of Na and Ca in zeolite's structure while cobalt shows a preference for Fe-rich sites. Correspondingly, it is clear that Langmuir and Freundlich isotherms and -parameters are of merely empirical character in the complex sorption system and cannot adequately represent the chemical processes of sorption competition. Therefore, the model code PhreeqC (pH redox equilibrium) based on the thermodynamic equilibrium such as geochemical processes of mineral dissolution and precipitation, ion exchange, surface sorption, aqueous complexation as well as redox reactions was applied in combination with the custom, Python based, inverse modelling tool P^3R, to adjust adsorption constant for individual ion interactions with zeolite [35–37]. Two types of ion exchange sites were considered: X^- and Y^-

Reactions

XNa: exchangeable for Cs^+, Ca^{2+}, Co^{2+}, Fe^{2+}

$$XNa + Cs^+ \rightarrow XCs + Na^+; \log\_k = -0.25$$

$$2\,XNa + Ca^{2+} \rightarrow X_2Ca + 2\,Na^+; \log\_k = -2.50$$

$$2\,XNa + Co^{2+} \rightarrow X_2Co + 2\,Na^+; \log\_k = -3.50$$

$$2\,XNa + Fe^{2+} \rightarrow X_2Fe + 2\,Na^+; \log\_k = -3.50$$

Sorption affinities X: Na > Cs > > Ca > Co = Fe.

Y_2Fe: exchangeable for Co^{2+} only

$$Y_2Fe + Co^{2+} \rightarrow Y_2Co + Fe^{2+}; \log\_k = -2.20$$

Sorption affinities Y: Fe > > Co.

The experimental sorption data with model simulations are presented in Fig. 6 for the experiments 1–5 with different concentrations where circles represent experimental data and lines represent the models (dark blue: Cs-sorption in single solutions, green: Co-sorption in single solutions, light blue: sorption in binary solutions).

The effect of competing ions is shown in Fig. 7. The presence of Ca^{2+}-ions in the solution resulted in a decrease of metal uptake especially in the case of cesium due to antagonistic effects during the adsorption.

Environmental compatibility tests by the TCLP method revealed that the percentage of cesium and cobalt in the leachate averaged 14.2% and 9.5% respectively. These findings are comparable with relevant literature data showing that the desorption rate of cesium and cobalt from the Petrota zeolite is low and therefore the material can be safely disposed in the environment [25, 38].

SEM–EDS and autoradiography investigation

SEM–EDS analyses were performed before and after Cs- and Co-sorption onto zeolite, using samples from the pristine zeolitic rock and zeolite in powder form. Figures 8a-b show images of the pristine zeolite rock in low and higher magnification along with the area and points where EDS analyses were performed. A dense clear layering structure (Fig. 8a) and aggregates with finer grains of zeolite can be observed (Fig. 8b). The chemical composition (in weight %) was presented in Table 1 and agrees with literature data for heulandite. Minor differences were observed after sorption in the binary system as it is shown in Fig. 8c and d. EDS analysis at various sites confirmed the presence of cesium (Cs: 0.5–2.2%). Cobalt was detected in lesser concentration as compared to cesium (Co: 0.2–0.7%) and detected in regions of high iron (Fe: 7–30%) concentration. The backscattered SEM images of the Petrota zeolite in powder form are given in Fig. 9a and b where separate particles of plate-like shape, and microaggregates, characteristic of monoclinic minerals are visible. Bright signal corresponds to regions with high concentrations of iron (up to 35%). Figure 9c shows the SEM image of the sample after Co-sorption where a different depict is observed with a plate like morphology. The percentage of cobalt ranged between 2.7 and 4.3%. Another illustration is exhibited by the corresponding zeolite sample after sorption of Cs/Co in Fig. 9d. The presence of cobalt (ca. 1.1%) was confirmed by EDS analysis in the bright spots with significant iron contents (31.3%) whereas cesium percentage up to 3.2% was detected.

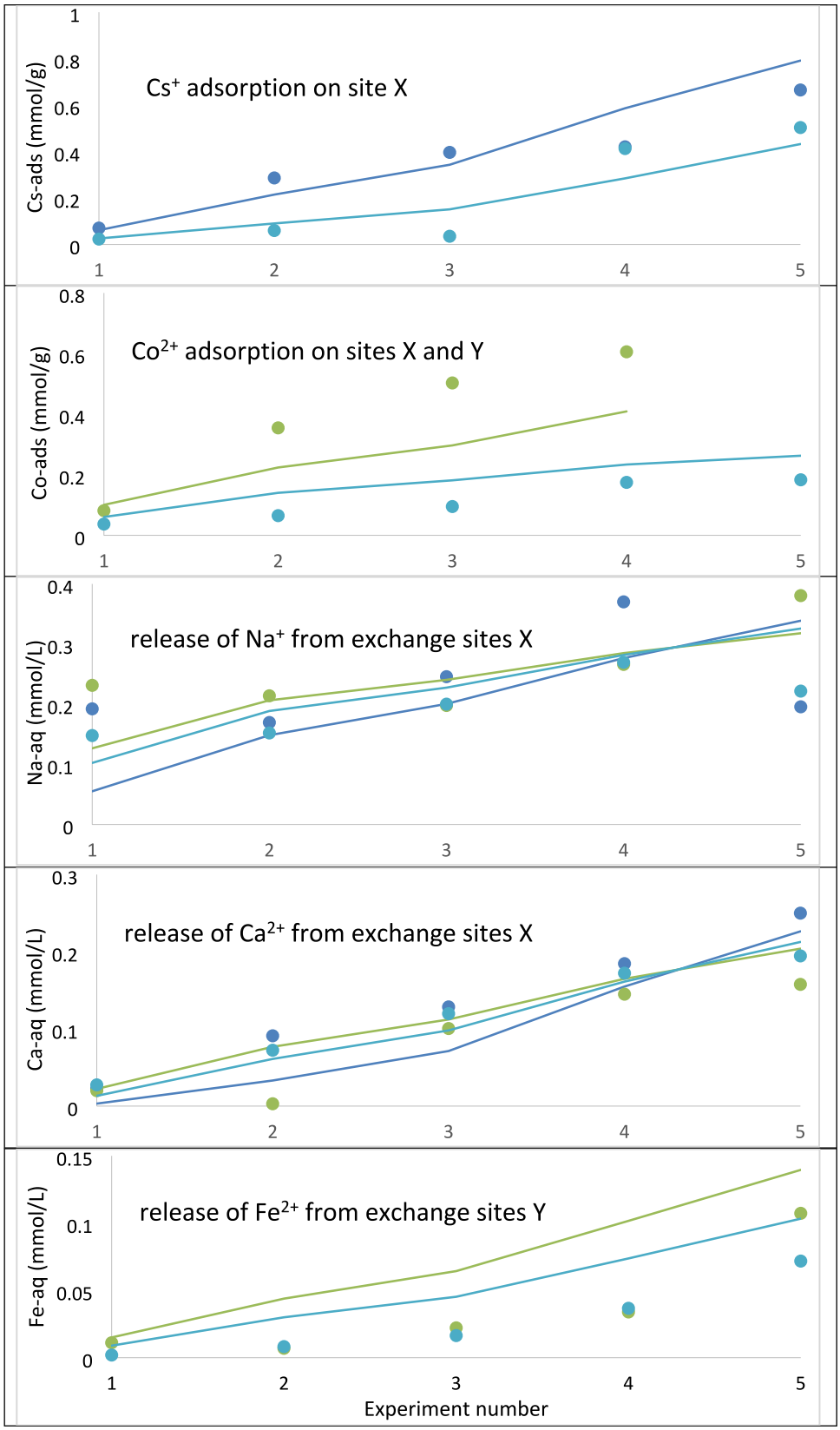

Fig. 6 Simulation data using the model code PhreeqC

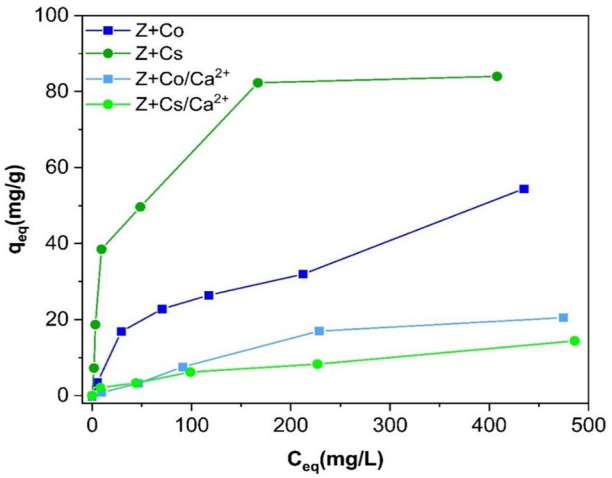

Fig. 7 Sorption isotherms in absence and presence of 0.05 mol L^{-1} $Ca(NO_3)_2$ (pH: 8, T: 295 K)

Furthermore, the detection of radiation of the sorbed radiocesium and radiocobalt on the zeolitic rock surface through autoradiography revealed information about the spatially distribution of the studied radionuclides. This technique provides visualization of the spatial distribution of the porosity and the field heterogeneities [39]. A fraction of initially sorbed ^{137}Cs and ^{60}Co onto zeolite stone, measured by autoradiography along with the EDS maps is shown in images of Fig. 10 (where cyan color is representative for K distribution). Low activity is displayed in blue to green, medium in yellow and high activity in red color. Comparisons of the images and activity distributions determined by autoradiography showed that the adsorbed activity was not necessarily correlated with the size and the location of the visible cracks, but among others, related to the overall microstructure and porosity of the zeolite as well as Fe-rich areas of the sample as was demonstrated from the SEM–EDS analysis.

Figure 11 shows the SEM image from a region of the sample before Co-sorption with the corresponding EDS analyses where different mineral phases can be seen such as cracks (yellow color) with high iron content (up to 25%) or regions rich in K and Na (light blue color), Ca (blue and green color) and Si-Al (red color).

HEU-type zeolites with an aperture 4.4–7.2 Å contain a large number of adsorption sites and selectivity to Cs^+ due to its hydrated ion radius of 3.29 Å. As reported in literature, cesium can penetrate and replace internal cations (Na^+, Ca^{2+}) of zeolite by ion-exchange in a wide range of conditions [25]. The uptake of Co^{2+} is less favored due to its bigger hydrated ion radius (4.23 Å) [40]. On the other hand, the sorption onto minerals is also influenced by particle size, mineralogical composition and impurities.

In this research work we confirmed the above findings via mathematical modeling of isothermal data supported by FTIR and SEM–EDS results. The fast sorption process, the effect of competitive ions and the metals release indicated that the Cs- and Co-sorption on the Petrota zeolite is governed mainly by ion exchange. The significant adsorption capacity of 81.3 mg g^{-1} for cesium and 63.7 mg g^{-1} for cobalt is due not only to its high CEC but also to its mineralogy composition [6, 10, 12, 41–44]. As mentioned before, cobalt was detected by SEM–EDS in iron-rich sites [41]. Iron, cobalt, and nickel belong to transition elements and are similar in properties. Concerning the competitive sorption of cesium and cobalt in binary systems it was revealed that the Cs-sorption was less affected by Co-sorption, which is consistent with the preferential uptake of cesium by clay minerals and also due to the mechanism of ion exchange which is the dominant mechanism especially in the case of cesium sorption. The specific sorption behavior of different elements and the effect of mineralogy composition on the retention of radionuclides as well as the simultaneous sorption of two or more metals in multicomponent systems is of great significance in the management of radioactive waste in real conditions and should be studied thoroughly in the future [42, 43].

Conclusions

This research provides insights concerning the factors that influence the sorption of cesium and cobalt on HEU-type zeolite such as particle size, CEC, specific surface area, mineralogical composition and impurities.

The XRD results showed that the crystallinity of the zeolite remains after the interaction with Cs, Co or Cs/Co solution and revealed small changes attributed to metal ion exchange. The characterization by FTIR also pointed out slight differences in the loaded materials.

SEM–EDS study and autoradiography tests showed the spatial distribution of Cs- and Co-loaded adsorbents in single and multicomponent systems which is affected by the mineralogy composition and the presence of different phases.

The sorption process was very fast and was influenced by the presence of competitive ions. The adjustment of the

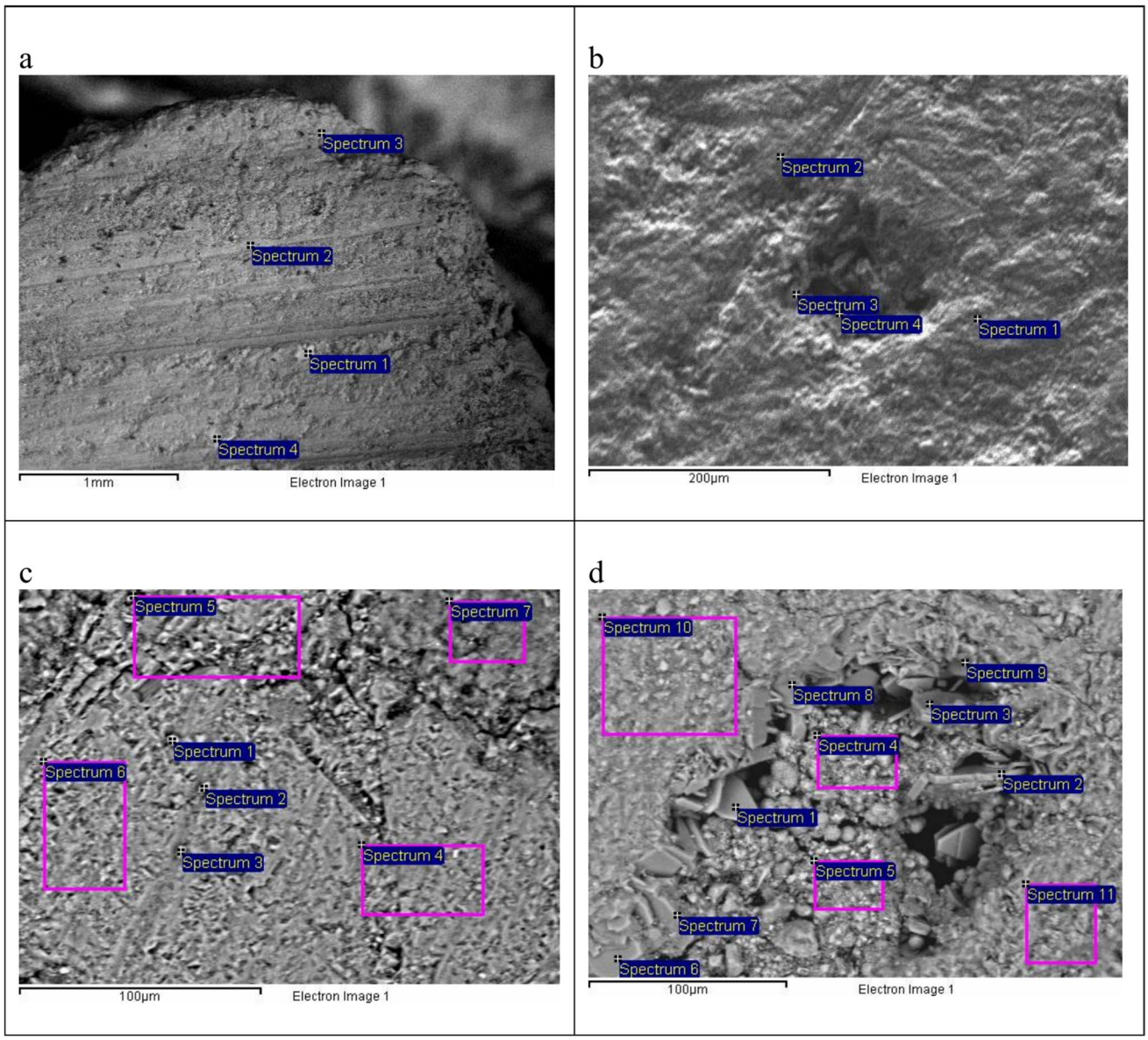

Fig. 8 SEM (backscattered electron) images for: (**a**), (**b**) pristine zeolitic rock and (**c**), (**d**) pristine zeolitic rock after Cs/Co-sorption

isothermal sorption data to Langmuir and Freundlich models showed significant sorption capacity (Q_{max}:81.3 and 63.7 mg g^{-1} for cesium and cobalt respectively).

Regarding the sorption results and the metals release into the solution after adsorption as well as the competitive binding of cesium and cobalt, a simple two site ion-exchange model was proposed which can be considered as the dominant adsorption mechanism in this research.

Environmental compatibility tests showed that the desorption rate of cesium and cobalt from the Petrota zeolite is low demonstrating the safe disposal of the material.

The obtained results provide useful information about the adsorption properties of HEU-type zeolites which will help in the application of these minerals as promising sorbents.

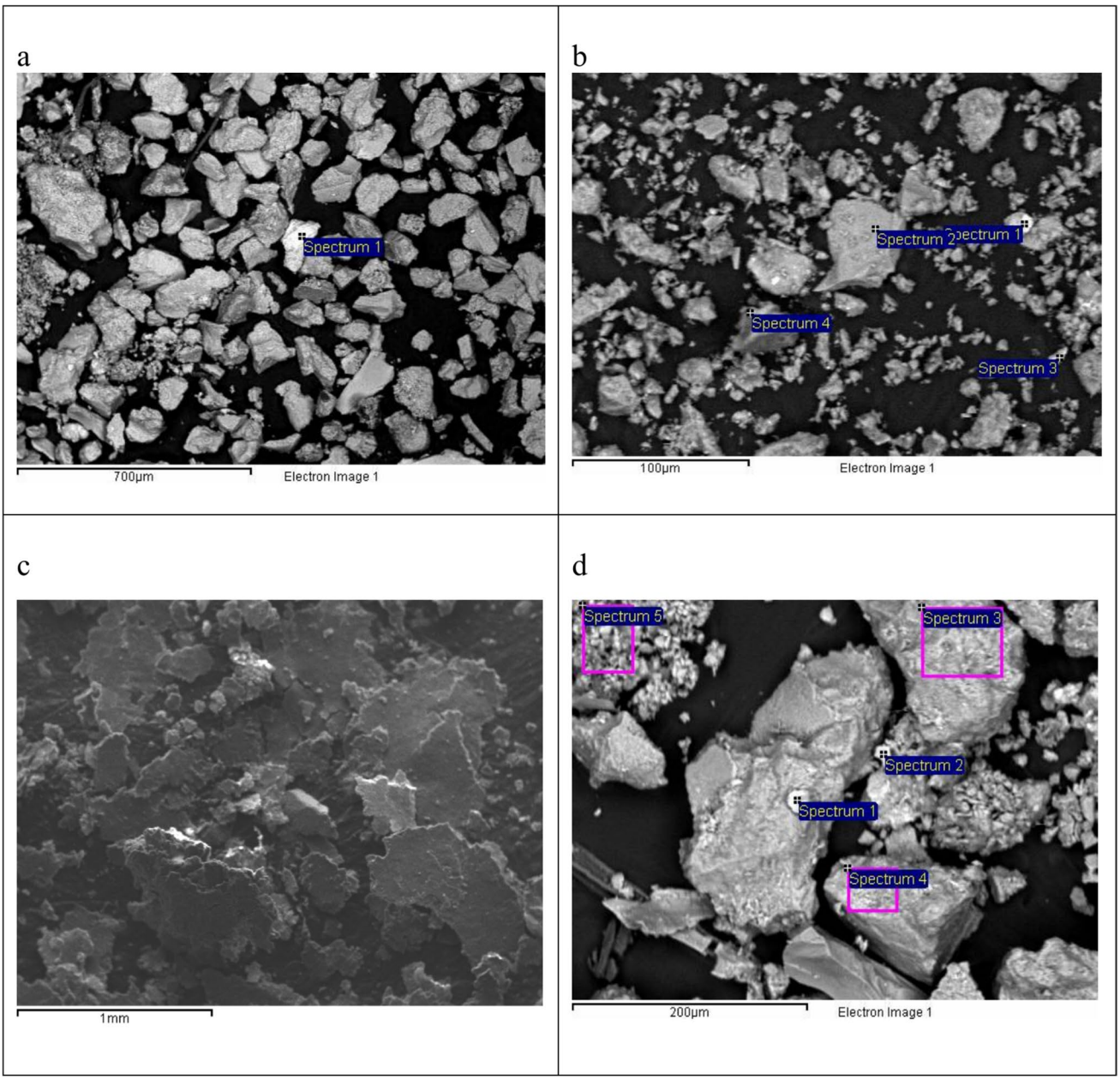

Fig. 9 SEM images for: (**a**), (**b**) zeolite (powder), (**c**) zeolite after Co-sorption, and (**d**) zeolite after Cs/Co-sorption in binary system

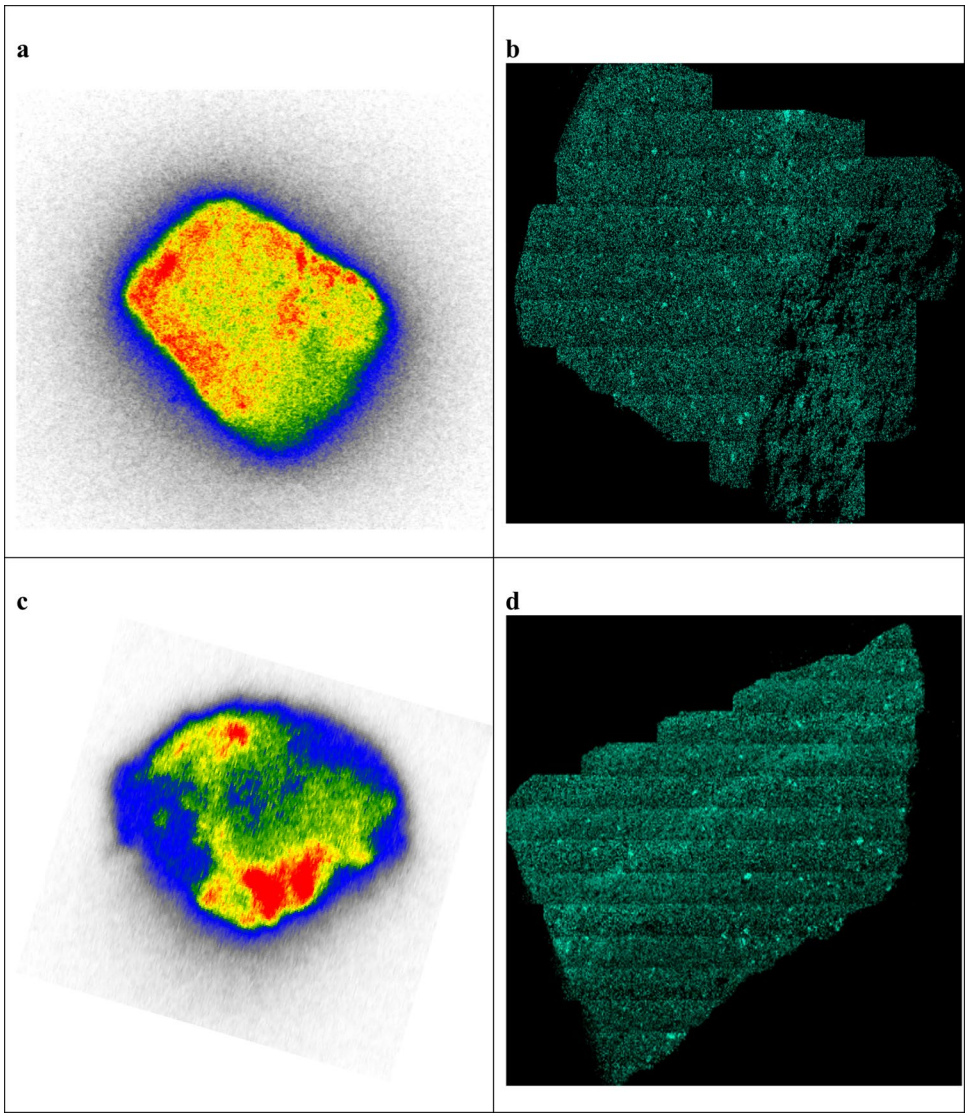

Fig. 10 Autoradiography images with the coresponding EDS maps: (**a**) zeolite loaded with ^{137}Cs, (**b**) pristine zeolitic rock, (**c**) zeolite loaded with ^{60}Co and (**d**) pristine zeolitic rock

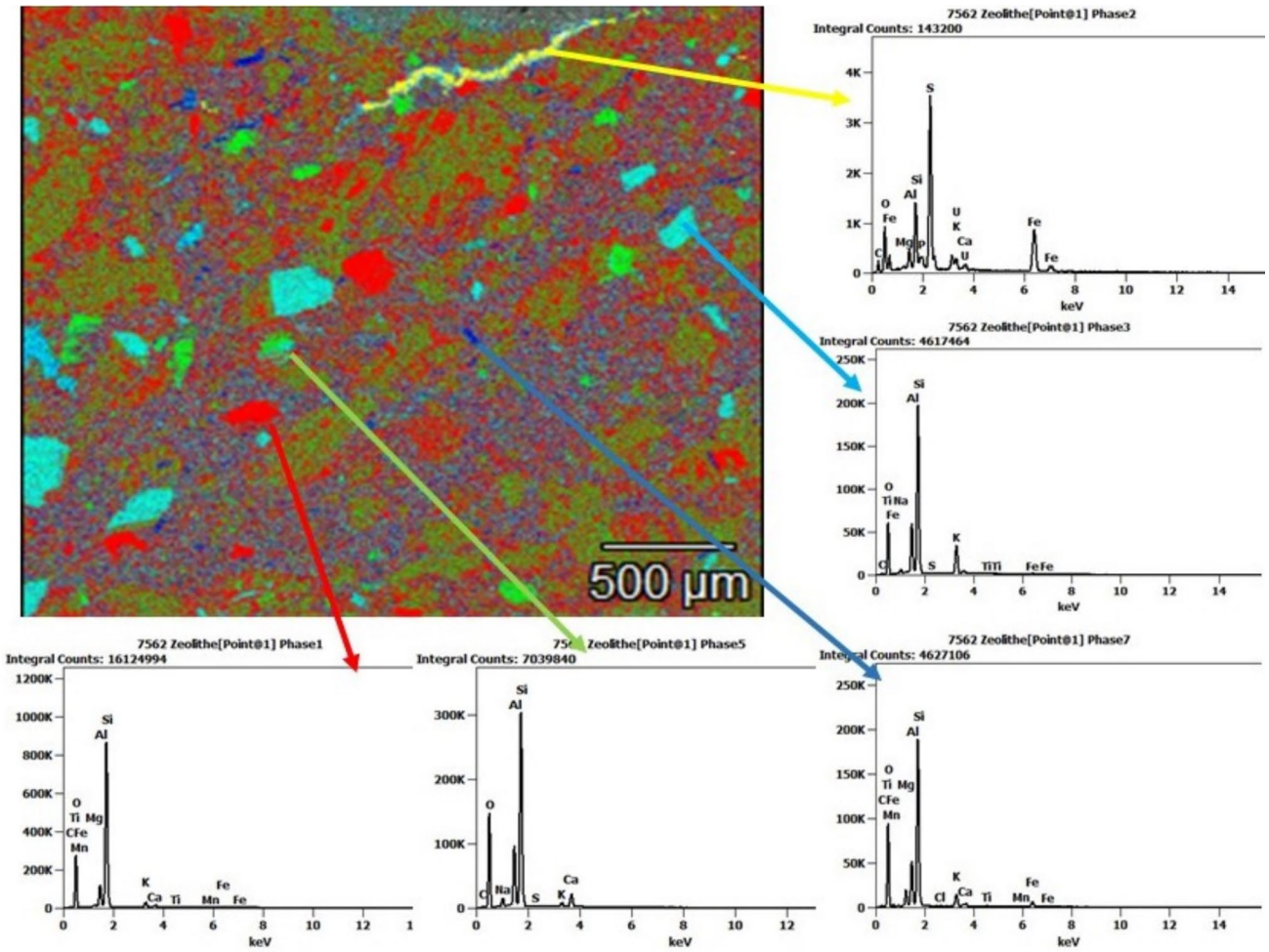

Fig. 11 SEM image and EDS analyses of the pristine zeolitic rock before Co-sorption

Acknowledgements Part of the study was performed during the research stay of the corresponding author (F.N.) within the KIT-International Excellence Fellowship Program at the Institute for Nuclear Waste Disposal of the Karlsruhe Institute of Technology (INE–KIT). The funding by KIT and the hospitality during this stage is gratefully acknowledged. The authors would also like to thank Stephanie Kraft and the group of ICP-OES (INE-KIT) and Eleftheria Kapashie and the group of SEM-EDS and XRD laboratories (AUTh) for help with the examination of the samples.

Funding Open access funding provided by HEAL-Link Greece.

Declarations

Conflict of interest No conflicts of interest were disclosed. The authors declare that there is no competing financial interest.

References

1. Misaelides P (2019) Clay minerals and zeolites for radioactive waste immobilization and containment: a concise overview. In: Mercurio M, Sharkar B, Langella A (eds) Modified clay and zeolite nanocomposite materials: environmental and pharmaceutical applications. Elsevier, Amsterdam, pp 241–261
2. Bish, D L (1989) Evaluation of past and future alterations in tuff at Yucca Mountain, Nevada, based on the clay mineralogy of drill cores USW G-1, G-2, and G-3: Technical Report. OSTI. GOV 60670
3. Keheyan Y, Khachatryan S, Christidis G, Moraetis D, Gevorkyan R, Sarkisyan H, Yeritsyan H, Nikoghosyan S, Sahakyan A, Kekelidze N, Akhalbedashvili L (2005) Sorption

behaviour of Armenian natural zeolites. Fusion Sci Technol 48:230–233
4. Kabuba J (2021) Selectivity of clinoptilolite towards heavy metals from industrial wastewater: equilibrium, kinetic, thermodynamic and elution studies. Eng Lett 29:158–167
5. Jiménez-Reyes M, Almazán-Sánchez PT, Solache-Ríos M (2021) Radioactive waste treatments by using zeolites. A short review. J Environ Radioact 233:106610
6. Rodríguez A, Sáez P, Díez E, Gómez JM, García J, Bernabe I (2018) Highly efficient low-cost zeolite for cobalt removal from aqueous solutions: characterization and performance. Environ Prog Sustain Energy 38:S352–S365
7. Shahwan T, Erten HN (2002) Thermodynamic parameters of Cs^+ sorption on natural clays. J Radioanal Nucl Chem 253:115–120
8. Yıldız B, Erten HN, Kıs M (2011) The sorption behavior of Cs^+ ion on clay minerals and zeolite in radioactive waste management: sorption kinetics and thermodynamics. J Radioanal Nucl Chem 288:475–483
9. Wang J, Zhuang S (2019) Removal of cesium ions from aqueous solutions using various separation technologies. Rev Environ Sci Biotechnol 18:231–269
10. Yu Lonin A, Levenets VV, Omelnik OP, Shchur AO (2021) Use of sorbents composition (clinoptilolite and synthetic zeolite) for elimination of cesium and cobalt from aqueous solutions. J Radioanal Nucl Chem 329:135–140
11. Noli F, Fedorcea V, Misaelides P, Cretescu I, Kapnisti M (2021) Cesium and barium removal from aqueous solutions in the presence of humic acid and competing cations by a Greek bentonite from Kimolos Island. Appl Radiat Isot 170:109600
12. Dianellou I, Karantoumanis F, Tsamos P, Noli F (2023) The effect of irradiation on the Cs, Co and Eu-removal from aqueous solutions using Greek minerals. J Radioanal Nucl Chem 332(6):1923–1933
13. Filippidis A, Kantiranis N, Tsirambides A (2016) The mineralogical composition of Thrace zeolitic rocks and their potential use as feed additives and nutrition supplements. Bull Geol Soc Greece L:1820–1828
14. Gutierrez M, Fuentes HR (1993) Modeling adsorption in multicomponent systems using a Freundlich-type isotherm. J Contam Hydrol 14:247–260
15. Park Y, Shin WS, Choi SJ (2012) Removal of Co, Sr and Cs from aqueous solution using self-assembled monolayers on mesoporous supports. Korean J Chem Eng 29:1556–1566
16. Park Y, Shin WS, Choi SJ (2012) Sorptive removal of cobalt, strontium and cesium onto manganese and iron oxide-coated montmorillonite from groundwater. J Radioanal Nucl Chem 292:837–852
17. MEDUSA (Make Equilibrium Diagrams Using Sophisticated Algorithms) (1983) I. Puigdomènech, INPUT, SED, and PREDOM: computer programs drawing equilibrium diagrams. Report TRITA-OOK-3010, Royal Institute of Technology (KTH), Dept. Inorg. Chemistry, Stockholm, Sweden
18. Limousin G, Gaudet JP, Charlet L, Szenknect S, Barthes V, Krimissa M (2007) Sorption isotherms: a review on physical bases, modeling and measurement. Appl Geochem 22:249–275
19. Lagergren S (1898) Zur theorie der sogenannten adsorption geloesterstoffe. Kungl Sven Vetenskapsakad Handl 24:1–39
20. Freundlich H (1906) Adsorption in solution. Phys Chem Soc 40:1361–1368
21. Wang J, Guo X (2020) Adsorption isotherm models: classification, physical meaning, application and solving method. Chemosphere 258:127259
22. Liu Y, Liu YJ (2008) Biosorption isotherms, kinetics and thermodynamics. Sep Purif Technol 61:229–242
23. Toxicity Characteristic Leaching Procedure. Washington, DC. (1992) https://www.epa.gov/hw-sw846/sw-846-test-method-1311-toxicity-characteristic-leaching-procedure. Accessed 30 May 2024
24. Elaiopoulos K, Perraki Th, Grigoropoulou E (2010) Monitoring the effect of hydrothermal treatments on the structure of a natural zeolite through a combined XRD, FTIR, XRF, SEM and N_2-porosimetry analysis. Microporous Mesoporous Mater 134:29–43
25. Belousov SA, Egorova T, Romanchuk A, Zakusin S, Dorzhieva O, Tyupina E, Izosimova Y, Tolpeshta I, Chernov M, Krupskaya V (2019) Cesium sorption and desorption on glauconite, bentonite, zeolite, and diatomite. Minerals 9(625):1–17
26. Filippidis A, Kantiranis N, Stamatakis M, Drakoulis A, Tzamos E (2007) The cation exchange capacity of the Greek zeolitic rocks. BGSG 40(2):723–735
27. Byrappa K, Suresh Kumar BV (2007) Characterization of zeolites by infrared spectroscopy. Asian J Chem 19:4933–4935
28. Mozgawa W (2000) The influence of some heavy metal cations on the FTIR spectra of zeolites. J Mol Struct 555:299–304
29. Krol M, Mozgawa W, Jastrzebski W (2016) Theoretical and experimental study of ion exchange process on zeolites from 5–1 structural group. J Porous Mater 23:1–9
30. Sobalík Z, Dědeček J, Ikonnikov I, Wichterlová B (1998) State and coordination of metal ions in high silica zeolites. Incorporation, development and rearrangement during preparation and catalysis. Micropor Mesopor Mater 21:525–532
31. Sobalík Z, Tvaružková Z, Wichterlová B (1998) Monitoring of skeletal T-O–T vibrations of metal ion exchanged zeolites. An attempt at quantitative evaluation. Microporous Mesoporous Mater 25:225–228
32. He M, Zhu Y, Yang Y, Han B, Zhan Y (2011) Adsorption of cobalt(II) ions from aqueous solutions by palygorskite. Appl Clay Sci 54:292–296
33. Fan X, Xue Q, Liu S, Tang J, Qiao J, Huang Y, Sun J, Liu N (2021) The influence of soil particle size distribution and clay minerals on ammonium nitrogen in weathered crust elution-deposited rare earth tailing. Ecotoxicol Environ Saf 208:111663
34. Dávila-Rangel JI, Solache-Ríos M (2006) Sorption of cobalt by two Mexican clinoptilolite rich tuffs zeolitic rocks and kaolinite. J Radioanal Nucl Chem 270:465–471
35. Parkhurst D-L, Appelo C-A-J (2013) Description of input and examples for PHREEQC version 3: a computer program for speciation, batch-reaction, one-dimensional transport, and inverse geochemical calculations. U.S. Geol Survey Tech Methods 6(A43):497
36. Heberling F, Klačić T, Raiteri P, Gale JD, Eng PJ, Stubbs JE, Gil-Díaz T, Begović T, Lützenkirchen J (2021) Structure and surface complexation at the calcite (104)–water interface. Environ Sci Technol 55:12403–21241
37. Machesky ML, Ridley MK, Heberling F, Lützenkirchen J (2023) Proton uptake at the barite-aqueous solution interface: a combined potentiometric, electrophoretic mobility, and surface complexation modeling investigation. ACS Earth Space Chem 7:1713–1726
38. Hamoud MA, Abo-Zahra SF, Attia MA, Someda HH, Mahmoud MR (2023) Efficient adsorption of cesium cations and chromate anions by one-step process using surfactant-modified zeolite. Environ Sci Pollut Res 30:53140–53156
39. Liang X, Wang F-Y, Zhang L, Zhang J-W, Wei C-S, Fan Y, Guo X-Z, Zhou T-F, Zhang J-Q, Lü Q-T (2023) Cobalt distribution and enrichment in skarn iron deposits: a case study of the Zhuchong skarn iron deposit, Eastern China. Ore Geol Rev 163:105778
40. Godelitsas A, Armbruster T (2003) HEU-type zeolites modified by transition elements and lead. Microp Mesop Mater 61(1–3):3–24
41. Gaboreau S, Prĸt D, Tinseau E, Claret F, Pellegrini D, Stammose D (2011) 15 years of in situ cement–argillite interaction from

Tournemire URL: characterisation of the multi-scale spatial heterogeneities of pore space evolution. Appl Geochem 26:2159–2171
42. Erdem E, Karapinar N, Donat R (2004) The removal of heavy metal cations by natural zeolites. J Colloid Interface Sci 280:309–314
43. Pipíška M, Florková E, Nemeček P, Remenárová L, Horník M (2019) Evaluation of Co and Zn competitive sorption by zeolitic material synthesized from fly ash using ^{60}Co and ^{65}Zn as radioindicators. J Radioanal Nucl Chem 319:855–867
44. Ballová S, Pipíška M, Frišták V, Ďuriška L, Horník M, Kanuchova M, Soja G (2020) Pyrogenic carbon for decontamination of low-level radioactive effluents: simultaneous separation of ^{137}Cs and ^{60}Co. Prog Nucl Energy 129:103484